AGU PUBLICATIONS

Space Weather

RESEARCH ARTICLE
10.1002/2016SW001471

What if we had a magnetograph at Lagrangian L5?

Alexei A. Pevtsov[1,2], Luca Bertello[1], Peter MacNeice[3], and Gordon Petrie[1]

[1]National Solar Observatory, Boulder, Colorado, USA, [2]ReSoLVE Centre of Excellence, Space Climate Research Unit, University of Oulu, Oulu, Finland, [3]Goddard Space Flight Center, NASA, Greenbelt, Maryland, USA

Key Points:
- Data from a magnetograph at Lagrangian L5 point will result in significant differences in forecasted (WSA-ENLIL) solar wind speed
- Data from L5 will affect PFSS model outcome in respect to areas of opened field and orientation of large-scale magnetic field neutral lines

Correspondence to:
A. A. Pevtsov,
apevtsov@nso.edu

Citation:
Pevtsov, A. A., L. Bertello, P. MacNeice, and G. Petrie (2016), What if we had a magnetograph at Lagrangian L5?, *Space Weather*, *14*, 1026–1031, doi:10.1002/2016SW001471.

Received 14 JUL 2016
Accepted 22 OCT 2016
Accepted article online 29 OCT 2016
Published online 10 NOV 2016

Abstract Synoptic Carrington charts of magnetic field are routinely used as an input for modelings of solar wind and other aspects of space weather forecast. However, these maps are constructed using only the observations from the solar hemisphere facing Earth. The evolution of magnetic flux on the "farside" of the Sun, which may affect the topology of coronal field in the "nearside," is largely ignored. It is commonly accepted that placing a magnetograph in Lagrangian L5 point would improve the space weather forecast. However, the quantitative estimates of anticipated improvements have been lacking. We use longitudinal magnetograms from the Synoptic Optical Long-term Investigations of the Sun (SOLIS) to investigate how adding data from L5 point would affect the outcome of two major models used in space weather forecast.

1. Introduction

Knowledge of the magnetic field in the solar photosphere plays an essential role in modern space weather forecasting. For example, synoptic maps of radial magnetic field are used as input for the Wang-Sheeley-Arge (WSA)-ENLIL model [*Arge and Pizzo*, 2000; *Odstrčil et al.*, 2002] to derive the properties of solar wind near the Earth and elsewhere in the solar system. The same type of maps are also employed in extrapolating the large-scale magnetic fields from the photosphere to the corona using, for example, potential field source surface (PFSS) model [see *Petrie*, 2013, and references therein]. Recently, full vector field synoptic maps became available from the Synoptic Optical Long-term Investigations of the Sun (SOLIS) and its Vector Spectromagnetograph (VSM) [e.g., *Balasubramaniam and Pevtsov*, 2011], which stimulated the use of nonlinear force-free field (NLFFF) modeling of global magnetic fields [e.g., *Tadesse et al.*, 2014]. Topology of magnetic field around the source regions of flares and coronal mass ejections (CMEs) offers important clues about orientation of magnetic field in interplanetary magnetic clouds and ejecta, and the information about large-scale magnetic connectivity in the solar corona brings better understanding of remote triggering solar eruptions [e.g., *Pevtsov*, 2012, and references therein]. However, modern synoptic maps are created using observations from a single Earth-facing viewing point (i.e., ground-based instruments on Earth or at Lagrangian L1). The synoptic maps capture the evolution of solar magnetic fields as they move across the visible ("nearside") solar hemisphere. Any changes that occur on the "farside" are not correctly represented by these synoptic maps. Some evolution of magnetic field on the farside could be represented via a flux transport modeling, by applying known differential rotation, supergranular diffusion, and the meridional flows. Emergence of new active regions could also be modeled by inserting bipolar flux elements at the locations determined from the helioseismic technique doubted farside imaging. This approach has been pursued in the framework of the Air Force Data Assimilative Photospheric Flux Transport (ADAPT) model [*Arge et al.*, 2010, 2011; *Hickmann et al.*, 2015].

The verification of model predictions is done via a direct comparison with observations: for example, parameters of solar wind from WSA-ENLIL model are compared with in situ observations from ACE or WIND spacecrafts [e.g., *Arge and Pizzo*, 2000; *Riley et al.*, 2013; *Jian et al.*, 2014]. PFSS model predictions of areas of opened field lines are contrasted with EUV and soft X-ray observations of coronal holes (e.g., Solar Dynamics Observatory/Atmospheric Imaging Assembly (SDO/AIA) or Hinode/X-ray Telescope-XRT [*Petrie and Haislmaier*, 2013]). Such comparative studies are often used to demonstrate strength or deficiency of a particular model or an observing station. Here we take a different approach and compare output of WSA-ENLIL and PFSS models computed using different input data. The goal of this exercise is to explore a hypothetical scenario, i.e., how the existence of additional data from the Lagrangian L5 point would benefit the modeling of solar corona and solar wind.

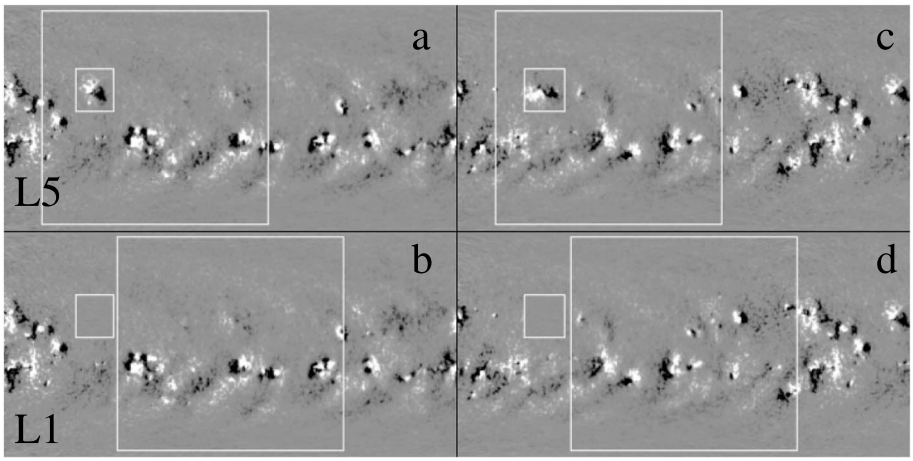

Figure 1. Near-real-time Carrington synoptic maps corresponding to the Lagrangian (a and c) L5 and (b and d) L1 viewing points. Large white boxes mark approximate range of latitudes and longitudes visible from each viewing point. Small white boxes are drawn around two isolated active regions. The regions are present in L5 observations but are absent in L1 observations as at the time corresponding to each map, when the region was outside of solar disk visible from L1 viewing point. Two NRT synoptic maps shown in Figures 1a and 1b correspond to the 25th day from the beginning of the time series used in this article (region 1). Figures 1c and 1d correspond to day 46 (second active region).

2. Data and Models

To model the effect of having additional observations from the Lagrangian L5 point, we employ a set of 48 daily near-real-time (NRT) synoptic magnetograms created from SOLIS/VSM observations. The time period covered by these observations is 62 days, and it corresponds to Carrington rotations CR2146–2149. These maps were taken as the real distribution of magnetic flux on solar surface. Next, the maps were modified by removing magnetic flux corresponding to two isolated bipolar active regions (Case 1 and Case 2) when the regions were outside of range of solar longitudes visible from the L1 viewing point. The removed magnetic flux was replaced by random noise with amplitude and spatial parameters corresponding to areas of quiet Sun in corresponding magnetograms. These modified maps were considered as if they were observed from the Lagrangian L1 viewing point. Synoptic maps corresponding to a combination of the Lagrangian L5 and L1 viewing points retained both active regions. Figure 1 shows an example of two Carrington near-real-time synoptic maps as they would appear from the Lagrangian L1 (Figures 1b and 1d) and a combination of L1 and L5 data (Figures 1a and 1c). The same data set was used recently by *Weinzierl et al.* [2016], and the reader is referred to that article for a more detailed description of the data.

For modeling we employed the Wang-Sheeley-Arge (WSA)-ENLIL and the potential field source surface (PFSS) models as discussed in the following sections.

3. Effects of L5 Viewing Point on PFSS Modeling of Open Field Lines

To evaluate the difference in coronal large-scale magnetic fields computed with and without additional data from the Lagrangian L5 point, we used the PFSS model implemented at the National Solar Observatory/National Solar Observatory (NSO) [*Petrie*, 2013]. Figure 2 shows four NRT synoptic maps corresponding to our Case 1 (Figures 2a and 2b) and Case 2 (Figures 2c and 2d) that depict the areas of opened magnetic fields and a large-scale magnetic neutral line. These areas of open field indicate possible location of the coronal holes. Foot points of open field lines of positive/negative polarity are colored in red/blue. Dashed circles mark an approximate position of areas of opened polarity fields, which we would like to discuss now. For Case 1, open field lines associated with the coronal hole are present when one uses a magnetogram that includes both L1 and L5 observations, but they are absent in the model output when only L1 observations are used. The shape of the source surface neutral line (SSNL, thick black line) is also distorted in L1 model output (compare Figures 2a and 2b to below and left of the dashed circle). SSNL marks the apex locations of the tallest closed field trajectories in the PFSS solution; these closed field lines correspond to the streamer belt, representing the equatorial current sheet.

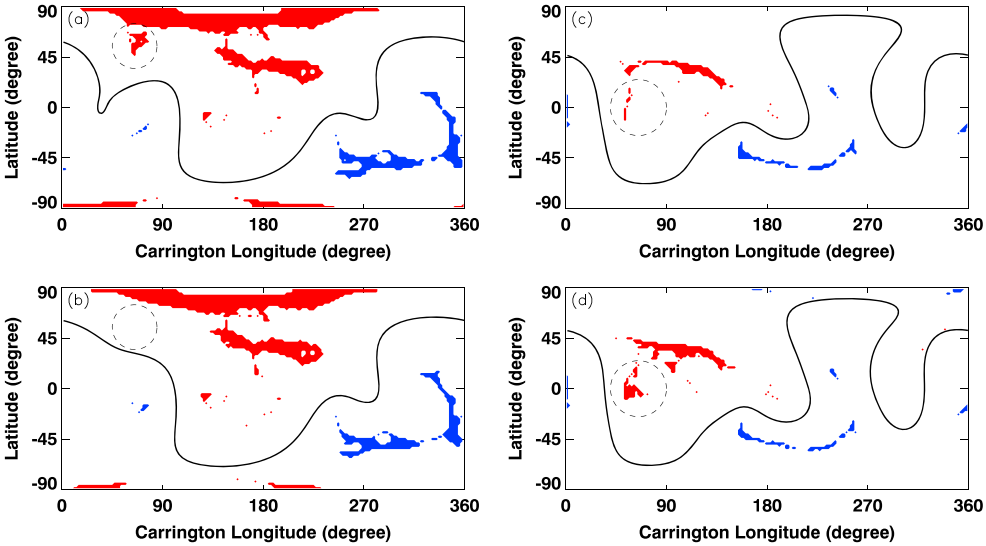

Figure 2. The results of PFSS modeling using data shown in Figure 1 as input for (a and c) L5 and (b and d) L1 viewing points. Blue and red colors mark areas of open magnetic flux of negative and positive polarity. The thick black line represents the magnetic neutral line of large-scale magnetic field (source surface neutral line, SSNL). Figures 2a and 2b correspond to Case 1 (removal active region 1), and Figures 2c and 2d are for Case 2. Dashed circles in Figures 2a and 2b outline position of an isolated coronal hole (open field lines), which is present in model realization based on L1 + L5 data (Figure 2a) but is absent when L1 data alone are used (Figure 2b). Figures 2c and 2d show Case 2, when the size of a coronal hole in model realization based on L1 data alone is significantly larger than in model predictions based on L1 + L5 data.

For Case 2 (Figures 2c and 2d), the size of isolated coronal hole is larger when only the data from L1 are used. In addition, the shape of the coronal hole situated above and to the right of the dashed circle is also slightly changed. Contrary to Case 1 (Figures 2a and 2b), in Case 2, the shape and the location of SSNL are not affected.

The difference between Case 1 and Case 2 suggests that lack of a small (magnetically closed) active region may have a different modeling outcome depending on large-scale topology of magnetic field in the vicinity of that region. In some cases, it could lead to appearance of an erroneous coronal hole, while in other cases it might result in erroneous reduction and maybe even a complete disappearance of the coronal hole that otherwise is present on the Sun. Such behavior is consistent with the notion of a global connectivity in solar corona on different spatial scales.

4. Effects of L5 Viewing Point on WSA-ENLIL Modeling of Solar Wind

To evaluate the difference in predicted parameters of solar wind with and without additional observations from Lagrangian L5 point, we used the WSA-ENLIL model (WSA V2.2 and ENLIL V2.7) that run at the Community Coordinated Modeling Center (CCMC), operated at NASA Goddard Space Flight Center. The WSA model allows predicting a quasi-steady flow of solar wind by employing the empirical relations between the magnetic field expansion factor and the solar wind speed. It uses a PFSS model to represent the magnetic fields at the source surface at about 2.5 solar radii, which is then linked to the Current Sheet Model (CSM, extends to 21.5 solar radii or 0.1 AU).

As described in *Pevtsov et al.* [2015], "the WSA code rebins the input synoptic maps to a surface grid of size 144 by 72 pixels, uniformly spaced in longitude and latitude with grid cell size of 2.5 degrees. The outer boundary of the current sheet component is placed at 21.5 solar radii (0.1 AU). The WSA solution on this spherical surface is used to provide the inner boundary condition for the ENLIL 3D MHD code. ENLIL uses a grid, uniformly spaced in spherical coordinates, of size 256 by 30 by 90 covering the domain from 0.1 to 2 AU in radius, 30 degrees to 150 degrees in polar angle (where 0 degrees is the solar north pole), and the full 360 degrees in longitude." For additional details on the WSA-ENLIL models and their implementation the reader is referred to *Arge et al.* [2004] and *Odstrcil et al.* [2008]. Figure 3 shows the time evolution of several parameters of solar wind relative to those as modeled by WSA-ENLIL. To simplify the comparison, we subtract the model predictions based on L1 data from the modeling based on (L1 + L5) data.

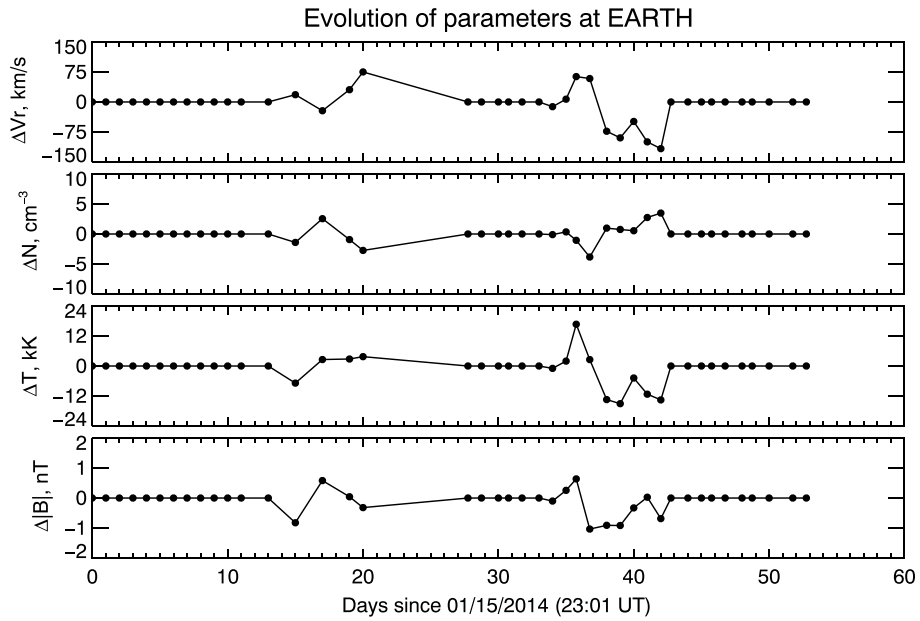

Figure 3. Output of WSA-ENLIL model showing (top to bottom) time variation of solar wind speed, electron density, temperature, and field strength at Earth. The plots show difference between the model predictions based on (L1 + L5) data and L1 data alone.

Prior to an active region 1 entering the field of view of instrument at L5 (Case 1, day 15 in Figure 3), the outputs of WSA-ENLIL model are identical for two inputs (L1 magnetograms alone and a combination of L1 and L5 data). However, when the active region 1 is included in L5 data, but is still absent from the L1 synoptic maps, we see significant deviations in all modeled parameters. In solar wind speed, the difference between two model realizations could reach 70–75 km s^{-1} (~20%). Electron density could differ by about 3 cm^{-3} (40%), and the magnetic field strength could change by about 1 nT (15%). Electron temperature appears to change by about 5 kK (10–15%). Between days 20 and 27, when the region enters the L1 viewing point, the differences between two model realizations disappear.

The effect of second active region (Case 2) is evident between days 34 and 43 (Figure 3). The amplitude of deviations is slightly larger as compared with Case 1: $\Delta V_r \approx 100-120$ km s^{-1} (~30%), $\Delta N \approx 3-4$ cm^{-3} (60–70%), $\Delta|B| \approx 1$ nT (20–25%), and $\Delta T \approx 15-20$ kK (45–50%).

The amplitude of changes in all parameters is larger than the uncertainties arising from evolution and observational noise of individual synoptic maps. Based on the ensemble modeling, *Pevtsov et al.* [2015] found that for Carrington rotation 2137, the scatter in parameters of solar wind predicted by WSA-ENLIL model is as follows: $\sigma(V_r) = 32$ km s^{-1}, $\sigma(N) = 1.52$ cm^{-3}, $\sigma(T) = 4.82$ kK, and $\sigma(|B|) = 0.55$ nT. The changes we see due to exclusion two active regions from L1 viewing point are larger than 1 σ uncertainties for all four parameters.

5. Discussion and Summary

Employing two widely used models (PFSS and WSA-ENLIL), we provide the quantitative estimates of the effect of observations from the additional (L5) viewing point on modeling of large-scale magnetic field in the corona and the properties of solar wind. We find significant differences in predicted location of areas of opened field lines (potential coronal holes) and orientation of neutral line of large-scale magnetic field. These differences occur in areas close to the location of small bipolar active regions that were removed from input magnetograms representing L1 viewing point. Away from these locations, the PFSS modeling outcome is less affected. In predicted solar wind properties, we find significant effects associated with the missing magnetic flux. The difference between the two model realizations (L1 observations alone and L1 + L5 data) is not as strong as the enhancements in solar wind properties associated with major interplanetary CMEs, but they are significantly larger than the uncertainties arising from the current input data. In case of two small (well-balanced) active regions, the difference between L1 and (L1 + L5) modeling prediction may reach 30% in solar wind speed, 60–70% in electron density, 20–25% in electron temperature, and 45–50% in magnetic

field strength. We speculate, however, that the difference could be more significant if a larger (by magnetic flux) active region had entered the L5 viewing point. We should stress that in this exercise, two model realizations were only compared with each other. We do not compare these model predictions with the heliospheric measurements.

While in the PFSS modeling the difference between L1 and (L1 + L5) results is limited to a vicinity of small active regions removed from the calculations for L1 viewing point, we expect that this could be a consequence of spatially limited differences between the two data sets. On the real Sun, the magnetic flux will change in other places, and thus, the difference in large-scale connectivity should also be expected. These large-scale effects were recently demonstrated by *Weinzierl et al.* [2016] using the same data set as this paper.

The PFSS and WSA-ENLIL models used in this exercise have several known problems. Thus, for example, PFSS model treats magnetic field above the solar photosphere as vacuum field (no gas pressure), and it also disregards the presence of electric currents known to exist from the magnetic field observations in the photosphere and the chromosphere. Alternative models do exist. For example, the current sheet source surface (CSSS) model [*Zhao and Hoeksema*, 1995] introduces additional "cusp surface" that allows for electric currents to ensure that the coronal fields at the outer boundary are purely radial and spatially uniformly distributed. Even more realistic are the full MHD models [*Feng et al.*, 2012a, 2012b]. The Magnetohydrodynamics Around a Sphere (MAS) model [*Mikić et al.*, 1999] is shown to successfully represent the solar corona as observed during the eclipses; it may also provide the basis for a more realistic modeling of solar wind [*Linker et al.*, 2016]. Still, PFSS and WSA-ENLIL models are widely used in research and the Space Weather Forecast and, thus, are quite suitable for such tests. While better estimates are possible with these more advanced models, our results provide the first quantitative evaluation of the importance of additional viewing point on forecasting the solar wind conditions at Earth location. With the limitations of models used in this test, perhaps, the reader should consider our results as the worse case scenario.

Acknowledgments
The authors thank anonymous reviewers for their thoughtful comments that led to the improvement of this paper. This work utilizes SOLIS data obtained by the NSO Integrated Synoptic Program (NISP), managed by the National Solar Observatory, which is operated by the Association of Universities for Research in Astronomy (AURA), Inc., under a cooperative agreement with the National Science Foundation. The data set of synoptic maps is available via http://dx.doi.org/10.7910/DVN/QVEE1N. This work benefited from the simulation results conducted by the Community Coordinated Modeling Center at Goddard Space Flight Center. The CCMC is a multiagency partnership between NASA, AFMC, AFOSR, AFRL, AFWA, NOAA, NSF, and ONR. A.A.P. acknowledges the financial support by the Academy of Finland to the ReSoLVE Centre of Excellence (project 272157).

References

Arge, C. N., and V. J. Pizzo (2000), Improvement in the prediction of solar wind conditions using near-real time solar magnetic field updates, *J. Geophys. Res.*, *105*, 10,465–10,480, doi:10.1029/1999JA000262.

Arge, C. N., J. G. Luhmann, D. Odstrcil, C. J. Schrijver, and Y. Li (2004), Stream structure and coronal sources of the solar wind during the May 12th, 1997 CME, *J. Atmos. Sol. Terr. Phys.*, *66*, 1295–1309, doi:10.1016/j.jastp.2004.03.018.

Arge, C. N., C. J. Henney, J. Koller, C. R. Compeau, S. Young, D. MacKenzie, A. Fay, and J. W. Harvey (2010), Air Force Data Assimilative Photospheric Flux Transport (ADAPT) model, in *Twelfth International Solar Wind Conference, AIP Conf. Proc.*, vol. 1216, edited by M. Maksimovic et al., pp. 343–346, Amer. Inst. of Physics Publishing, College Park, Md., doi:10.1063/1.3395870.

Arge, C. N., C. J. Henney, J. Koller, W. A. Toussaint, J. W. Harvey, and S. Young (2011), Improving data drivers for coronal and solar wind models, in *Numerical Modeling of Space Plasma Flows: ASTRONUM 2010, ASP Conf. Ser.*, vol. 444, edited by N. V. Pogorelov, E. Audit, and G. P. Zank, pp. 99–104, Astron. Soc. of the Pac., San Francisco, Calif. [Available at http://adsabs.harvard.edu/abs/2011ASPC..444...99A.]

Balasubramaniam, K. S., and A. Pevtsov (2011), Ground-based synoptic instrumentation for solar observations, in *Solar Physics and Space Weather Instrumentation IV., Proc. SPIE 8148*, edited by S. Fineschi and J. Fennelly, 814809, Society of Photo-Optical Instrumentation Engineers (SPIE), Bellingham, Wash., doi:10.1117/12.892824

Feng, X., C. Jiang, C. Xiang, X. Zhao, and S. T. Wu (2012a), A data-driven model for the global coronal evolution, *Astrophys. J.*, *758*, 62, doi:10.1088/0004-637X/758/1/62.

Feng, X., L. Yang, C. Xiang, C. Jiang, X. Ma, S. T. Wu, D. Zhong, and Y. Zhou (2012b), Validation of the 3D AMR SIP-CESE solar wind model for four Carrington rotations, *Sol. Phys.*, *279*, 207–229, doi:10.1007/s11207-012-9969-9.

Hickmann, K. S., H. C. Godinez, C. J. Henney, and C. N. Arge (2015), Data assimilation in the ADAPT photospheric flux transport model, *Sol. Phys.*, *290*, 1105–1118, doi:10.1007/s11207-015-0666-3.

Jian, L., P. J. MacNeice, A. Taktakishvili, R. M. Evans, D. Odstrcil, C. N. Arge, B. V. Jackson, H. S. Yu, P. Riley, and I. Sokolov (2014), Validation of coronal and heliospheric models for quasi-steady solar wind: WSA-Enlil, MAS-Enlil, SWMF, and IPS tomography models, Abstract SH33A-4118 presented at 2014 Fall Meeting, AGU, San Francisco, Calif., 15–19 Dec. [Available at http://adsabs.harvard.edu/abs/2014AGUFMSH33A4118J.]

Linker, J. A., R. M. Caplan, C. Downs, R. Lionello, P. Riley, Z. Mikic, C. J. Henney, C. N. Arge, T. Kim, and N. Pogorelov (2016), An empirically driven time-dependent model of the solar wind, *J. Phys. Conf. Ser.*, *719*, 012012, doi:10.1088/1742-6596/719/1/012012.

Mikić, Z., J. A. Linker, D. D. Schnack, R. Lionello, and A. Tarditi (1999), Magnetohydrodynamic modeling of the global solar corona, *Phys. Plasmas*, *6*, 2217–2224, doi:10.1063/1.873474.

Odstrčil, D., J. A. Linker, R. Lionello, Z. Mikic, P. Riley, V. J. Pizzo, and J. G. Luhmann (2002), Merging of coronal and heliospheric numerical two- dimensional MHD models, *J. Geophys. Res.*, *107*(A12), 1493, doi:10.1029/2002JA009334.

Odstrcil, D., et al. (2008), Numerical simulations of solar wind disturbances by coupled models, in *Numerical Modeling of Space Plasma Flows, ASP Conf. Ser.*, vol. 385, edited by N. V. Pogorelov, E. Audit, and G. P. Zank, pp. 167–173, Astron. Soc. of the Pac., San Francisco, Calif.

Petrie, G. J. D. (2013), Solar magnetic activity cycles, coronal potential field models and eruption rates, *Astrophys. J.*, *768*, 162–179, doi:10.1088/0004-637X/768/2/162.

Petrie, G. J. D., and K. J. Haislmaier (2013), Low-latitude coronal holes, decaying active regions, and global coronal magnetic structure, *Astrophys. J.*, *775*, 100, doi:10.1088/0004-637X/775/2/100.

Pevtsov, A. A. (2012), Complex magnetic evolution and magnetic helicity in the solar atmosphere, in *The Sun: New Challenges, Astrophys. and Space Sci. Proc.*, vol. 30, edited by V. N. Obridko, K. Georgieva, and Y. A. Nagovitsyn, pp. 83–91, Springer, Berlin, doi:10.1007/978-3-642-29417-4_8.

Pevtsov, A. A., L. Bertello, and P. MacNeice (2015), Effect of uncertainties in solar synoptic magnetic flux maps in modeling of solar wind, *Adv. Space Res.*, *56*(12), 2719–2726, doi:10.1016/j.asr.2015.05.043.

Riley, P., J. A. Linker, and Z. Mikić (2013), On the application of ensemble modeling techniques to improve ambient solar wind models, *J. Geophys. Res. Space Physics*, *118*, 600–607, doi:10.1002/jgra.50156.

Tadesse, T., T. Wiegelmann, S. Gosain, P. MacNeice, and A. A. Pevtsov (2014), First use of synoptic vector magnetograms for global nonlinear force free coronal magnetic field models, *Astron. Astrophys.*, *562*, A105, doi:10.1051/0004-6361/201322418.

Weinzierl, M., D. H. Mackay, A. R. Yeates, and A. A. Pevtsov (2016), The possible impact of L5 magnetograms on non-potential solar coronal magnetic field simulations, *Astrophys. J.*, *828*, 102, doi:10.3847/0004-637X/828/2/102.

Zhao, X., and J. T. Hoeksema (1995), Prediction of the interplanetary magnetic field strength, *J. Geophys. Res.*, *100*, 19–33, doi:10.1029/94JA02266.